MSE-MRI sequence optimisation for measurement of bi- and tri-exponential T2 relaxation in a phantom and fruit

Hans Adriaensen, Maja Musse, Stéphane Quellec, Alexandre Vignaud, Mireille Cambert, François Mariette

Corresponding Author: Dr Maja Musse, Ph.D.

Corresponding Author's Institution: IRSTEA

First Author: Hans Adriaensen, Ph.D.

Order of Authors: Hans Adriaensen, Ph.D.; Maja Musse, Ph.D.; Stéphane Quellec; Alexandre Vignaud, Ph.D.; Mireille Cambert; François Mariette, Ph.D.

ABSTRACT:

The transverse relaxation signal from vegetal cells can be described by multi-exponential behaviour, reflecting different water compartments. This multi-exponential relaxation is rarely measured by conventional MRI imaging protocols; mono-exponential relaxation times are measured instead, thus limiting information about of the microstructure and water status in vegetal cells. In this study, an optimised Multiple Spin Echo (MSE) MRI sequence was evaluated for assessment of multi-exponential transverse relaxation in fruit tissues. The sequence was designed for the acquisition of a maximum of 512 echoes. Non-selective refocusing RF pulses were used in combination with balanced crusher gradients for elimination of spurious echoes. The study was performed on a bi-compartmental phantom with known T_2 values and on apple and tomato fruit. T_2 decays measured in the phantom and fruit were analysed using bi- and tri-exponential fits, respectively. The MRI results were compared with low field non-spatially resolved NMR measurements performed on the same samples.

The results demonstrated that the MSE-MRI sequence can be used for up to tri-exponential T_2 quantification allowing for estimation of relaxation times from a few tens of milliseconds to over a second. The effects of the crusher moment and the TE value on T_2 measurements were studied both on the bi-compartmental phantom and on the fruit tissues. It was demonstrated that the sequence should be optimised with regard to the characteristics of the tissue to be examined by considering the effects of water molecular diffusion in the presence of both imaging gradients and gradients produced by susceptibility inhomogeneities.

1

1 Introduction

Quantitative Magnetic Resonance Imaging (MRI) measurements have been used in several studies to investigate vegetal tissues [1-2]. The transverse relaxation time (T_2) is known to be related to the water status in cell compartments, *i.e.* water content, water mobility and interactions between water and macromolecules [3]. T_2 mapping is an approach that is currently used in MRI studies and it has been demonstrated to be crucial for the attribution of physiological meaning to MRI images.

As with many biological tissues, plant tissues exhibit multi-exponential relaxation behaviour, the characterisation of which is important for investigation of tissue microstructure. Conventional MRI imaging protocols are rarely employed for investigation of multi-exponential relaxation; they are generally used to provide an approximate mono-exponential relaxation time. Despite this limitation, mono-exponential T_2 mapping has been used for investigation of fruit development [4], ripening [5] and technological processes such as pressure treatment [6] and freezing [7], demonstrating the dependency of the average T_2 on different transformation processes. However, this approach does not make it possible to investigate changes at the subcellular level, thus interpretation of physiological phenomena that occur in fruit tissues remains difficult.

On the other hand, non-spatially resolved NMR relaxation measurements allow access to subcellular information and thus provide a deeper analysis of water status and transfer inside vegetal cells. Changes in fruit produced by various processes have been studied by NMR. For example, Van der Weerd [8] studied water exchange through the permeable membrane between the compartments of maize cells. Both the ripening process [5,9], and the different transformation processes were analysed [10-11]. The main difficulties with NMR relaxometry stem from the fact that measurements are not spatially resolved and they require fruit

2

sampling. The latter can lead to erroneous measurements as disruption of fruit tissues produced by sampling can affect the results. Moreover, this technique does not provide the opportunity to follow individual fruit through physiological processes and thus is particularly unsuitable for biological samples characterized by wide diversity. On the other hand, localized multi-component T_2 measurements such as the SVS (single voxel selection) Carr-Purcell-Meiboom-Gill (CPMG) sequences [12] can be used to acquire multi-exponential T_2 relaxation. The drawback of this technique is that only a single voxel is studied and as the voxel should contain homogeneous tissue for accurate T_2 measurements its selection can be difficult. There is, therefore, a real need to develop MRI methods for multi-exponential T_2 mapping that allow measurements in individual fruit throughout a given process under investigation.

In the study presented here, an optimised Multiple Spin-Echo (MSE)-MRI sequence was evaluated for assessment of multi-exponential transverse relaxation in fruit tissues and the effects of the sequence parameters on T_2 measurements were demonstrated. Experiments were performed on a phantom exhibiting bi-exponential relaxation and on fruit. Because of the effects of the susceptibility inhomogeneities on the T_2 measurements, two different fruit tissues were investigated in all experiments: the tomato pericarp, as it is characterised by relatively low porosity, and the apple parenchyma, as it is known to contain a large number of air bubbles. Parallel to the MRI experiments, T_2 and relative signal intensity of the phantom solutions and of the fruit samples taken to match with the pixels used for T_2 computing from MRI images were measured by low-field NMR. The aim was to compare the MRI results with the low-field NMR measurements considered as the reference technique for multi-exponential T_2 and quantification of associated signal intensities. In fact, NMR measurements were performed in optimal experimental conditions with a large number of closely spaced sampling points, preventing any influence of diffusion effects and allowing accurate T_2 fitting. We,

therefore, considered NMR T_2 measurements as reference, and on the basis of these results we discuss trends in MRI results with regards to the imaging parameters and characteristics of the tissues under investigation. Both multi-exponential T_2 and relative signal intensities that reflect water distribution between cell compartments were analysed. Although the transverse relaxation time depends on the field strength due to the contribution of the chemical exchange, it was considered approximately constant over the B_0 range investigated in the present study (0.47 T and 1.5 T for NMR and MRI experiments, respectively), according to [13-14].

2 Theory

Multi-exponential relaxation in plant tissues is modelled by:

$$I(t) = \sum_i I_{0,i} \exp\left(-t/T_{2,i}\right) + const \qquad (1)$$

where t represents the time, and $I_{0,i}$ is proportional to the local spin density of the ith signal component and $T_{2,i}$ the transverse relaxation time of the ith signal component. Although other protons such as sugar protons may also contribute to signal density, it can be assumed that in fruit tissue $I_{0,i}$ reflects the water density.

As stated above, MSE-MRI sequences for T_2 measurements are often limited by relatively poor data. In addition to the problem of noise-sensitivity of data, the small number of echoes is not sufficient for sampling the complicated relaxation curves of biological tissues. A long echo train with a short Echo Time (TE) is required to cover the complete range of transverse relaxation times ranging from a few milliseconds to over a second. Extracting information regarding multi-T_2 components from standard commercial MRI sequences is,

therefore, questionable. Besides the sampling difficulties, the reliability of T_2 measurements depends on technical factors in the MRI sequence. The MSE sequences require 180° refocusing pulses, which are in practice far from ideal and are sensitive to inhomogeneities of both the Radio Frequency (RF) field (B_1) and static field (B_0) [15-16]. The consequence of pulse imperfection in a multi-echo sequence is the generation of spurious signals that result in image artefacts and in the introduction of T_1 dependence on the T_2 relaxation decay. The problem of stimulated echoes is amplified for long echo trains and closely spaced echoes. An overview of the practical problems of quantitative T_2 measurements involved in multiple echo MRI is provided by Poon *et al.* [17].

The classical method to reduce the image artefacts due to stimulated echoes is to apply a phase encoding gradient before each echo signal and to undo the phase encoding with a rewinding gradient before the subsequent 180° pulse. In this way, both stimulated and desired echoes are phase-encoded identically. This echo superimposition makes it possible to acquire artefact-free images but relaxation curves are still corrupted by stimulated echoes. One way to address the problem of stimulated signals is to use phase cycling methods [18]. The difficulty of this approach is that the number of repetitions required for effective phase cycling increases with the echo train and the acquisition time becomes long. Additionally, according to [17], phase schemas are ineffective for the case when phase encoding gradients are applied before the refocusing pulses. Nevertheless, several phase pathways using a limited number of phase cycles have been proposed [18], but unfortunately they eliminate only certain stimulated echoes and leave other components unaffected. Another method for elimination of stimulated echoes is to use crusher gradients around the 180° pulses in order to isolate the desired spin-echo pathway. This method has been demonstrated to be the most effective strategy for suppression of stimulated echoes in multi-echo imaging. Different crusher gradient patterns have been employed in previous studies [15,19] and their effectiveness has

been compared by Poon *et al.* [17]. The drawback with the use of crusher gradients is that any pulse imperfections lead to a constant cumulative loss of signal (*f*) from successive echoes [17] modelled by:

$$\frac{1}{T_{2_{appararent}}} = \frac{1}{T_{2_{intrinsic}}} + \frac{f}{TE} \tag{2}$$

where *f* depends on the flip angle and the type of refocusing pulse when T_2 values are long compared to TE. Eq. (2) is valid if -log(frf) = f where frf is the fraction of the signal refocused [20]. Eq. (2) demonstrates that the apparent decrease in relaxation time depends on the fractional signal loss and TE and is amplified for long T_2 values.

The limitations of both phase cycling and crusher gradient methods for stimulated echo elimination suggest the importance of the refocusing pulse that is employed. The difficulties caused by the selective refocusing pulses for T_2 quantification, along with the greater robustness of the hard pulse and especially of various composite pulses, have been demonstrated [15]. Despite this, it is important to note that multi-slice imaging requires a selective refocusing pulse and that the time course of composite pulses is longer than common hard pulses, increasing both TE and power deposition.

T_2 quantification is also affected by various T_2-reducing contributions. In this study, we take into account the effects of diffusion of water molecules in the presence of random field gradients generated by susceptibility inhomogeneities (T_2') and diffusion-acting imaging gradient pairs (T_2'') [13,21-22]:

$$\frac{1}{T_{2_{appararent}}} = \frac{1}{T_{2_{intrinsic}}} + \frac{1}{T_2'} + \frac{1}{T_2''} \tag{3}$$

The local field gradients contribute to the relaxation according to following model [23]:

$$\frac{1}{T_2'} \propto \gamma^2 \langle g_z^2 \rangle TE^2 D \tag{4}$$

where γ represents the nuclear gyromagnetic ratio, $\langle g_z^2 \rangle$ the mean square distribution of the local field gradients proportional to $B_0{}^2$ and D the self-diffusion constant of the molecules observed. Chemical exchange has similar effects on T_2', also in proportion to $B_0{}^2$ but with smaller and more complex dependence on TE [24]. The diffusion of water molecules in the presence of diffusion-acting imaging gradient pairs attenuates the MRI signal exponentially and can be modelled by [22] :

$$I_{n-1} = I_n \exp(-bD) \tag{5}$$

where I_{n-1} and I_n are signal intensity of successive echoes, and in the case of a pair of rectangular gradients b is given by:

$$b = \gamma^2 G^2 \delta^2 (\Delta - \frac{\delta}{3}) \tag{6}$$

where G is the strength of the rectangular gradient lobe, δ the duration of the gradient and Δ the distance from the gradient lobe centres. Unrestricted diffusion is assumed. The diffusion contribution in the signal relaxation is therefore generally provided by [22]:

$$\frac{1}{T_2''} = \frac{\gamma^2 G^2 \delta^2}{TE} \left(\Delta - \frac{\delta}{3} \right) D \tag{7}$$

7

For the specific case of readout gradients, Eq. (7) becomes [13]:

$$\frac{1}{T_2^"} = \gamma^2 G_{readout}^2 \delta'^2 \left(1 - \frac{4\delta'}{3TE}\right)D \qquad (8)$$

where $G_{readout}$ is the strength of the rectangular readout gradient lobe and $2\delta'$ the duration of the read gradient. Finally, T_2 quantification is also altered by the diffusion of water molecules in the presence of crusher gradients. As for readout gradients, crusher gradients (Fig. 2) can be seen as a train of pulse-field gradients and the diffusion contribution is described according to Eq. (7).

3 Materials and Methods

3.1 Phantom and Plant Material

3.1.1 Phantom

The phantom was manufactured in-house by drilling 9 holes in the sides of a cylindrical block of resin measuring 21 cm in diameter and 13 cm in height (Fig. 1 A). Four paramagnetic nickel sulfate ($NiSO_4$) aqueous solutions ($T_2 \sim T_1$) with T_2 of 32 ± 0 ms, 155 ± 1 ms, 596 ± 3 ms and 1392 ± 9 (values measured by NMR at 20 MHz, see section 2.3) were made to simulate the relaxation properties of fruit tissues [25-26]. In fact, multi-exponential T_2 values range from 20-30 ms to about 1600 ms in tomato and apple fruit tissues; with corresponding T_1 values from about 200 ms to about 1700 ms. The solutions were distributed into several compartments in order to generate a combination of six different bi-compartmental elements for MRI slices positioned as in Fig. 1 B. The solutions were arranged

8

according to their T_2 values (in ms) as follows: $[T_{2,\,long}/T_{2,\,short}]$ = [1392/596], [1392/155], [1392/32], [596/155], [596/32], and [155/32]. Note that the $[T_{2,\,long}/T_{2,\,short}]$ = [1392/32] ms combination was used twice, resulting in seven pairs of holes being filled so that each side of the phantom had a single-elemental response for the four different solutions.

3.1.2 Fruit

A batch of 5 ripe tomatoes (Admiro, provided by the Centre Technique Interprofessionnel des Fruits et Légumes (CTIFL, France)) and one of 6 ripe apples (Reine des Reinettes, purchased from the local market) were used in this study.

3.2 MRI

The MRI measurements were carried out on a whole-body 1.5 Tesla scanner (Magnetom Avanto, Siemens, Erlangen, Germany) with maximum imaging gradients of 40 mT/m. The MRI system was equipped with a single-element head coil to acquire data for the phantom and with an 8-channel knee receiver coil for data acquisition for the fruit.

3.2.1 MRI sequence

An MSE-MRI sequence allowing up to 512 echoes to be collected was developed (Fig. 2). To perform this, the changes in the commercial MRI sequence were achieved using the Siemens Integrated Development for Environment Application (IDEA).

Spin excitation was performed by a three-lobed sinc 90° pulse lasting 2.048 ms, while the refocusing pulse was a hard 180° pulse lasting 0.5 ms. The CPMG condition [27-28] was obtained by phase shifting the 180° refocusing pulses by 90° relative to the initial 90°

excitation pulse. Constant balanced slice and readout crushers were applied around each refocusing pulse. Phase encoding and rewinding gradients were applied around each echo rather than a single phase encoding step performed before the first refocusing pulse. As explained above, in the absence of any stimulated echoes, only single phase encoding can be used. However, our preliminary study showed that for long echo trains (512 echoes) the phase encoding/rewinding strategy is necessary for artefact-free images, which demonstrated that the problem of stimulated echoes was not entirely resolved even when large crushers were employed.

The timing parameters required for the fixed events (crusher gradients and ramp-time delays) of the sequence were optimised to give the shortest TE possible for a given bandwidth (BW).

In the sequence developed, the choice of the crusher moment, the refocusing pulse type and other common parameters could be set via the standard user interface.

3.2.2 MRI experiment

The temperature of the thermally-insulated Faraday cage was set at 19°C and monitored during measurements; deviations were found to be less than 0.8°C. The fruit to be investigated were placed in the Faraday cage at least 3 hours and the phantom at least 24 hours before the beginning of the experiment, thus guaranteeing and maintaining a constant and homogeneous temperature of the objects during the MRI measurements.

Fruit were marked prior to the MRI experiment, making it possible to take samples for NMR measurements from the same selected slice. The image slices corresponded in all cases to the equatorial region of the fruit.

The mono-exponential relaxation study in the phantom was performed by selecting the MRI slice to correspond to one range of compartments, while for the bi-exponential relaxation

study, the MRI slice was selected to include both compartment ranges at a 50%-50% ratio (see Fig. 1 B).

The MRI data of the phantom were collected with the MSE sequence with the following geometrical parameters: Field Of View (FOV) 15.2^2 cm^2, matrix size 128^2 and slice thickness (ST) 10 mm. The median equatorial plane of each fruit was imaged with a FOV of 13.6^2 cm^2, matrix size of 112^2 and ST 8 mm. The BW was 260 Hz/pixel, the Repetition Time (TR) was 10 s, and 512 echoes were acquired in all experiments. The images were acquired with 2 averages, resulting in total imaging times of about 43 and 37 min for the phantom and the fruit, respectively.

The experimental optimisation of the MSE sequence parameters was performed first on the phantom and then on the fruit. The latter was crucial mostly because fruit have porous tissues and thus the effects of diffusion throughout gradients generated by susceptibility inhomogeneities were intensified. The focus of interest here was the investigation of the effects of (1) the crusher moment and (2) the TE value on T_2 and associated signal intensity measurements. The experiments consisted of the following:

1. Images were acquired with crusher moments of 0, 5, 25 and 50 x 10^{-6} T.s/m; with TE = 12 ms. TE was set at its minimum value for the least favourable case (crusher moment of 50 x 10^{-6} T.s/m). The momentum was changed by varying the gradients lengths and keeping the amplitude maximal.

2. Images were acquired with TE of 7.1, 9.1 and 12 ms, with a crusher moment of 5 x 10^{-6} T.s/m.

The multi-exponential T_2 and corresponding relative signal intensities were computed from the image series according to Eq. (1) and compared to the reference NMR measurements. One tomato and one apple were used in the optimisation study and three samples from each fruit were examined by NMR.

Once the optimisation study had been performed, the experimental protocol defined by it was applied on the fruit batches in order to validate the T_2 and the corresponding relative signal intensity measurements. As in the optimisation study, three samples were taken from each fruit for NMR analysis.

3.2.3 Image processing

The regions of interest (ROI) comprising seven compartments or seven pairs of compartments, depending on whether mono- or bi-exponential relaxation was studied in the phantom, were selected and the mean value of the ROIs were computed for all the MSE amplitude images of the series. In the case of fruit, three ROIs in the homogeneous parts of the outer pericarp and the parenchyma for tomatoes and apples were analysed, respectively. This mean ROI signal was then fitted via the Levenberg-Marquardt criterion for chi-square minimisation by means of TableCurve2D software, using bi- and tri-exponential functions [see Eq. (1)] for the phantom and the fruit, respectively. Scilab software based on the Levenberg-Marquardt algorithm was used to produce pixel-by-pixel fitting, thus generating T_2 maps. ROIs identical to those used in the first approach were selected in the T_2 maps and the mean values of T_2 and relative signal intensities were compared to those obtained by the ROI-based method.

3.3 NMR relaxometry

The NMR measurements were performed on a 20 MHz spectrometer (0.47 T, Minispec PC-120, Bruker, Karlsruhe, Germany) equipped with a thermostated probe.

The fruit samples for the NMR experiments were taken to match with the ROIs used for T_2 computed from MRI images. The latter was very important for comparison of the NMR

and MRI results. The sampling protocol consisted of cutting an 8 mm thick slice at the equatorial region of the fruit that corresponded to the MRI slice, subsequently cylinders of 8 mm in diameter were cut out of the outer pericarp and parenchyma of tomatoes and apples, respectively, at the same locations as the MRI ROIs were drawn. Samples were gently wiped to remove water from the broken cells and then placed in NMR tubes which were closed with caps.

T_2 was measured using the Carr-Purcell-Meiboom-Gill (CPMG) sequence: successive echoes were recorded with a 90°-180° pulse spacing of 0.5 ms. Data were averaged over 8 and 16 acquisitions for the phantom and the fruit tissues, respectively. A Recycle Delay (RD) was adjusted for each sample to avoid saturation of the magnetisation. Thus, for the solutions with T_2 values of 32, 155, 596 and 1392 ms, the RD were set at 1, 2, 5 and 12 s and the corresponding numbers of points were 1000, 2000, 5000 and 12000, respectively. For the tomato and apple samples the RD were set at 12 s and 10 s, respectively, and the corresponding numbers of points were 12000 and 10000, respectively, Measurements were performed at 19°C (same temperature as for the MRI measurements) once the temperature had stabilised within the sample.

NMR T_2 relaxation curves were fitted by Scilab software according to two different methods, the Maximum Entropy Method (MEM) [29], which provides a continuous distribution of relaxation components without any assumption concerning their number, and the Levenberg-Marquardt algorithm which allows a discrete solution for fitting the curve.

4 Results

4.1 NMR measurements

As expected from previous studies [25,30], the optimum fitting of the T_2 relaxation signal for both tomato and apple tissues was achieved by a four-exponential function independently of whether the fitting method was discrete (Levenberg-Marquardt algorithm) or continuous (MEM). Only the results of discrete fitting are presented in following sections. The mean T_2 values and corresponding relative signal intensities of all measurements performed on the tomatoes and apples are given in Table 1A.

4.2 Optimisation of MRI T_2 measurements in phantom

4.2.1 Crusher effects

As expected, the MRI images of the phantom contained artefacts (Fig. 3A) when no crushers were applied. Typical artefacts due to simulated echoes occurred [18] in the form of a mirror ghost image and a wavelike variation in image intensity in the phase-encoded direction across the image. By applying crushers in the acquisition sequence, the artefacts were removed (Fig. 3B). The signal of a mono-exponential T_2 decay of the solution with $T_2 = 1392$ is shown in Fig. 3C to provide a quantitative representation of these artefacts. In the case of images acquired in the absence of crushers, the T_2 decay had an oscillating behaviour and the baseline was higher than for the T_2 decay measured with the same sequence in the presence of crushers.

Fig. 4 shows the effects of crusher moment on the I_0 and T_2 values computed for mono- and bi-exponential T_2 relaxation. In the case of the mono-exponential relaxation (Fig. 4A), the intensity of the crusher moment did not influence the signal intensity whatever the T_2

values of the solutions probed. On the other hand, the signal intensity generally tended to be slightly higher for solutions with shorter T_2. The same phenomenon of I_0 dependency on T_2 value was observed in the case of the bi-exponential relaxation, although the average relative intensities computed for different solution combinations were very close to 50%-50% (Fig. 4C). As in the case of mono-exponential relaxation, no influence of the crusher moment on signal intensity was observed.

The effect of crusher moment on the measured T_2 values is shown in Fig 4B and D. As expected, T_2 values obtained with the MRI-MSE imaging sequence were shorter than the reference NMR values, principally due to the effects of the diffusion signal attenuation in the presence of imaging gradients. The chemical exchange effects were considered to be minor over the range of B_0 used, however, as the measurements were performed at different magnetic field strengths, they could slightly influence the transverse relaxation times. Concerning crusher effects, the T_2 of two shorter T_2 solutions (T_2 of 32 and 155 ms, NMR values) were constant in terms of the full range of crusher moments explored for both mono- and bi-exponential relaxation (26±0 ms and 126±1 ms). The T_2 of the third solution (NMR T_2 of 596 ms), decreased slightly with increasing crusher moment, while the T_2 of the longest T_2 solutions (T_2 = 1392 ms, NMR value) decreased significantly. The effects of crusher moment on the T_2 values measured can be explained by the diffusion of the water molecules in the presence of crusher gradients. As indicated in the Introduction, the crusher gradients also act as diffusion gradients and thus the diffusion weighting increases according to crusher moment, mainly affecting long T_2 values. The phenomenon described was estimated for our experiment from Eq. (7), by taking into account the diffusion throughout crusher gradients only, and for D = 2.1 x 10^{-9} $m^2.s^{-1}$ which is the diffusion coefficient for water at 20° C. In this case, the theoretical decreases in the T_2 values for increases in the crusher moment from 5 x 10^{-6} Ts/m to 50 x 10^{-6} Ts/m were expected to be 24%, 12%, 3% and 1% for the T_2 (NMR

values) equal to 1392 ms, 596 ms, 155 ms and 32 ms, respectively, with $T_{2\text{-}intrinsic}$ approximated to the NMR value. A very similar trend was observed in the experimental results (19%, 9%, 2% and 0%) for the T_2 (NMR values equal to 1392 ms, 596 ms, 155 ms and 32 ms, respectively). On the other hand, no effect of crusher gradients on the signal intensity was seen in the range of the crusher moments studied.

4.2.2 TE effects

Fig. 5 shows the effects of TE on the I_0 and T_2 values computed for mono- and bi-exponential T_2 relaxation. As in previous experiments, the signal intensity generally tended to be slightly higher for solutions with shorter T_2. The signal intensities of the mono-exponential relaxation remained unchanged for TE values from 7.1 until 9.1 ms and slightly decreased at TE = 12 ms for the slowest relaxing T_2 component. Fig. 5C shows an example of the bi-exponential relaxation (T_2 = 155 and 1392 ms, NMR values). The expected approximate 50%-50% ratio was found at TE 7.1 ms and 9.1 ms, while a slight unbalance was noticed for TE = 12 ms (Fig. 5A).

The effect of TE on the T_2 values measured was not observed in the range of TE studied (Fig 5B and D). Theoretically, the dependence of the T_2 measurements on TE is multiple. It is related to i) to the effects of pulse refocusing imperfection [see Eq. (2)]; ii) the diffusion of water molecules throughout the readout gradients [see Eq. (8)] and iii) the diffusion of water molecules in the presence of the gradients generated by susceptibility inhomogeneities [see Eq. (4)]. The estimation from Eq. (8) showed that the molecular diffusion in the presence of readout gradients did not influence T_2 measurements for the experimental conditions used, as the highest decrease in T_2 values occurring for the longest T_2-component was expected to be less than 1%. Similarly, the effects of pulse imperfection should be attenuated by increasing the TE for a given f, inducing an increase in T_2, but this

was not observed for the experimental parameters used. Finally, susceptibility effects in the phantom solutions that were considered to be almost free of air bubbles were also negligible. Note that an increase in TE can also affect the accuracy of measurements for the shortest T_2 component because of insufficient sampling of the relaxation curve. This effect was insignificant for the solutions used in this study.

4.3 Optimisation of MRI T_2 measurements in fruit tissues

As shown in section 4.1, fitting of the NMR T_2 relaxation decays was achieved by a four-exponential function for both tomato and apple tissues. On the other hand, fitting of MRI data to a four exponential function was not reliable, as the MRI sequence provided a lower number of more spaced echoes than NMR. The optimum fitting of the MRI T_2 relaxation curves was achieved by a tri-exponential function for both tomato and apple tissues. Because NMR relaxation times were used as reference values for comparison with MRI results, the fast relaxing NMR components were excluded from analysis in the subsequent investigation. We assumed that observation of this component in the MRI experiments was hindered by its short relaxation time and by the small contribution that it provided to the overall MRI signal measured.

4.3.1 Crusher effects

As in the phantom, T_2 values measured in fruit tissues by the MRI-MSE imaging sequence were shorter than by NMR but the T_2 decrease was amplified, especially for the slowest relaxing components. It can also be observed that the decrease in T_2 was more pronounced in apple tissues. On the other hand, the relative signal intensities were distributed

slightly differently, the slowest relaxation component being underestimated compared to the NMR results. This was particularly noticeable for apple tissues.

As in the phantom experiments, the shorter MRI T_2 compared to NMR values were explained by diffusion of the water molecules in the presence of imaging gradients. However, in the case of fruit tissues the gas in intercellular spaces gave rise to local differences in magnetic field gradients. Molecular diffusion throughout these gradients additionally affected the results, especially for the relatively porous apple parenchyma tissue [31], leading to the greater difference between the results of the MRI and NMR measurements. The local field gradients also explain the differences in the relative intensities measured with two techniques [24].

The relative signal intensities of the three components were fairly similar for the three values of crushers investigated in both the tomato and apple tissues (Figs. 6A and C). No obvious tendency was demonstrated for T_2 values (Figs. 6B and D), except that the T_2 of the slowest relaxation component for tomato tissues decreased slightly for the crusher moment of 50×10^{-6} T.s/m. Both results concerning I_0 and T_2 were consistent with the results of the phantom measurements. As observed in the phantom experiments, I_0 was not sensitive to changes in crusher gradient moment for the range of values applied. $T_{2\text{-}intrinsic}$ approximation with the NMR value was no longer applicable when a decrease in T_2 due to susceptibility effects occurring in fruit tissues was taken into account. The decrease in T_2 due to crusher gradients was therefore not computed from theoretical equations for the slight decrease occurring for the long T_2 in both tomato and apple tissue.

4.3.2 TE effects

The relative intensity of all T_2 components (Fig. 7A) remained constant with increasing TE values in the tomato tissue, while it changed in the apple tissue (Fig. 7C). The relative intensity of the slowest-relaxing component decreased, and consequently the opposite

18

was demonstrated for the two shorter components, according to the results obtained from non-imaging relaxation studies [24]. On the other hand, the T_2 values of all components decreased with increasing TE for both types of fruit (Fig. 7B and D). Furthermore, as for I_0, the effects of TE on the T_2 values measured were more pronounced for apple than for tomato tissue.

Comparing the results from the phantom and fruit measurements, it is apparent that TE effects on I_0 and T_2 values depended strongly on the tissues observed. In the case of phantom measurements, the TE effects were almost negligible for TE between 7.1 ms and 12 ms, while they were distinct in the case of fruit, especially apples. This supported the hypothesis that the effects are mainly due to diffusion of the water molecules in the presence of gradients produced by susceptibility inhomogeneities.

4.4 T_2 MRI-NMR relationship – phantom and fruit results

It was shown in the above section that the optimum parameters for the MSE-MRI sequence were a crusher moment of 5×10^{-6} Ts/m and a TE value of 7.1 ms. These parameters were used in combination with the settings described in section 2.2.2 for the validation experiment.

As already explained, the results for the phantom and the fruit T_2 measurements were analysed using bi- and tri-exponential fitting procedures, respectively. Fig. 8 A, B and C depicts examples of the ROIs drawn on the T_2-weighted images of the phantom and fruit obtained by the MSE sequence. The ROIs contained 124 and 21 pixels, for phantom and fruit, respectively. The experimental points and fits of MRI decay T_2-curves of the mean signal of the ROIs are shown in Fig. 8 D. The signal intensities were found to decay from initial values near 1000 and 1600 for phantom and fruit, respectively, to values of around a few a. u. The standard deviation (sd) for ROIs placed in the image background was about 2.1 and 1.1 for phantom and fruit, respectively. For all the fits, the residuals were normally distributed, the

coefficient of determination r^2 was > 0.99 and fitting standard errors were about few percents of the estimated parameters. Note that it was the case for all the fits performed in this study (studies of TE and crusher moment effects). By changing the initial guess randomly, fits were found to be relatively insensitive to its value. The results of T_2 measurements performed in phantom and fruit are summarised in Table 2 and Table 1B, respectively.

The ratio between relative signal intensities of the two components measured in the phantom is represented in Fig. 9A, demonstrating a relatively low standard deviation (4%) from the mean 50% value. This result is very satisfactory, especially when the possible errors in phantom positioning are considered. The relationship between relative signal intensities of different components of tomato tissues (Fig. 9A) measured by MRI and NMR was approximated by a linear function. It can be seen that the relative signal intensity of the middle component was slightly overestimated compared to the relative signal intensity of the slowest relaxing component. The linear relationship for apple tissues was not established between relative MRI and NMR signal intensities. It was demonstrated above (see Fig. 7 C) that, in the presence of random gradients produced by susceptibility inhomogeneities, the effects of the diffusion of water molecules on the signal intensity observed depended on the intrinsic T_2 value. The relative intensities of longer T_2-components were therefore underestimated and in consequence the relative signal intensities of shorter T_2 components were overestimated. This can be clearly observed for apple tissues (Fig. 9 A). For tomato tissues, characterised by relatively low porosity, the linear relationship was described by a relatively high slope (0.97).

In terms of T_2 values, the relationships between MRI and NMR T_2 values were found to be linear for the phantom (Fig. 9B), with a slope of 0.89. For apple tissue, this relationship could also be approximated by a linear function, with a considerably lower slope. In the case of tomato tissues, T_2 underestimation of the slowest relaxing component was particularly

noticeable because of the longer T_2 values (NMR value close to 1500 ms) and the relationship between MRI and NMR T_2 values could not be considered as linear. These results showed that the relationship between the MRI and NMR T_2 values depends both on intrinsic T_2 values and on the characteristics of the tissue studied. However, despite T_2 compression, the MRI sequence used allowed to measure accurately the different T_2 components.

It can also be seen from Fig. 9 that more scattering occurred for the tomato results than in the apple results. This was probably due to the fact that the samples taken for NMR measurements were more homogeneous in the apple parenchyma than in the outer tomato pericarp. Indeed, small fractions of surrounding locular tissues might be contained in the NMR samples.

4.5 T_2 maps in phantom

As described above, T_2 and I_0 maps of the phantom were generated by fitting the amplitude images on a pixel-by-pixel basis using the corresponding bi-exponential function (Fig. 10). These maps allowed assessment of the spatial distribution of two different T_2 components and their associated relative signal intensities. The ROI-based parameters and the parameters averaged on the pixel-by-pixel maps gave remarkably similar results. Not even 1% difference could be demonstrated for either the T_2 or the signal intensity parameters, thus validating the robustness of the T_2 maps.

The relatively high SNR of fruit images ($I_{first-echo}/sd_{noise} \sim 1400$) was sufficient to resolve tri-exponential relaxation on an ROI-basis but probably not high enough for reliable computation of relaxation parameter maps. The simulations showed that the fitting procedure was sensitive to the initial parameters. Consequently, T_2 maps were not computed for the fruit tissues.

5 Discussion

Separation of multi-exponential T_2 components in commercial MRI scanners is limited by signal-to-noise ratio, echo spacing and echo train length. This is especially the case for fruit tissues, as the T_2 of different cell compartments ranges from a few milliseconds for water associated with the cell wall to over a second for water in the vacuole. A long echo train and short echo time are therefore needed to cover the complete T_2 range. The present study demonstrated that it is possible to characterise multi-exponential transverse relaxation with the optimised MSE 512echo-imaging sequence. The problem of the generation of stimulated echoes that result in image artefacts and the modulation of the amplitude image in subsequent echoes that occurs in the MSE sequences with such a large number of sampling points was addressed by the application of crusher gradients and the use of non-selective rectangular refocusing pulses.

With the use of crusher gradients, any imperfection in the RF refocusing pulse due to B_1 and B_0 inhomogeneities leads to constant signal loss and therefore affects the T_2 measurements. The decrease in T_2 depends on both the refocusing pulse and the echo spacing used [see Eq. (2)] Since the bias introduced by the imperfection in the RF refocusing pulse decreases with increasing echo spacing, the undesired effects can theoretically be reduced by using long echo times. The latter effect was not observed in the range of TE investigated. Nevertheless, maximising the echo spacing is not an alternative when short relaxation times are measured, and especially when tissues of interest have a structure that may cause susceptibility inhomogeneities. Sled *et al.* [32] proposed a method for correcting variations in B_0 and B_1 by applying rectangular and composite RF refocusing pulses. This approach is applicable to multi-component relaxation studies and will be considered in our future investigations. A multi-component fitting algorithm for simulated echo correction proposed recently by Prasloski et al. [33] can also be considered in future investigations. It would be

interesting to consider the analyse of the trade-off of echo spacing and bandwidth for the characterisation of the tri-pool system with characteristics similar to those of fruit systems, like the analysis demonstrated by Dula et al. [34], although this approach does not take into account the problems related to spin diffusion and refocusing pulse imperfections.

Crusher gradients also act as diffusion gradients, and elimination of diffusion weighting affecting T_2 measurements is therefore not possible. The effects of the crusher moment on T_2 measurements were investigated in this study, and showed dependency of the T_2 observed on these imaging gradients. The optimal crusher moment value was the minimum value at which artefacts disappeared. As expected from the theory, the diffusion effects affected the relaxation times and were especially noticeable for long T_2 values. The decrease in the T_2 values with an increase in the crusher moment observed experimentally matched well with the trend predicted from Eq. (7), which shows that the MSE-MRI results can to some extent be corrected for given experimental conditions.

The decrease in T_2 due to diffusion in the presence of readout gradients was not observed in the present study. This is explained by the medium pixel resolution of the images (here 1.2 mm), because readout gradients act as diffusion gradients, especially at high pixel resolution in the readout direction. The most obvious effects on T_2 and the associated relative signal intensity components measured at 1.5 T magnetic field were due to the diffusion of water molecules in the presence of random field gradients generated by susceptibility inhomogeneities. TE effects were hardly distinguishable in the phantom experiments, while any increase in TE in fruit tissues resulted in an underestimation of the T_2 values, especially for apple tissues. Moreover, the relative signal intensities were also affected in apple tissues, demonstrating that accurate T_2 estimations in porous fruit tissues can only be performed for short echo spacing.

As described above, the imperfections in the RF refocusing pulse led to signal loss and to the underestimation of transverse relaxation time. Hard RF pulses provided better uniformity of the slice profile than selective pulses; rectangular refocusing pulses were therefore used, considering a single slice approach to be appropriate to study fruit tissues. The performance of the refocusing pulse can be further improved by using composite pulses instead of a rectangular pulse. However, a composite pulse is longer than a rectangular pulse and will thus increase the echo spacing, hence amplifying the effects of T_2 underestimation due to susceptibility inhomogeneities. Furthermore, using a composite pulse involves an increase in RF power deposition in the object and thus limits the number of echoes sampled on the relaxation curve.

Relaxation times and associated relative signal intensities measured by the low field non-spatially resolved NMR were used as reference values, as they were acquired in optimal experimental conditions of high numbers of echoes with short inter-echo spaces. On comparing the T_2 of aqueous solutions measured by MRI with NMR results, we found that the T_2 values and their associated relative intensities were in excellent agreement for the whole range of values studied (*ca.* 30 ms – 1400 ms). As expected, T_2 values obtained with the MRI-MSE imaging sequence were shorter than those obtained by NMR ($T_{2\text{-MRI}} = 0.89 T_{2\text{-NMR}}$) due to several points that have to be taken into account. Firstly, the two measurements were not performed at the same magnetic field and consequently the chemical exchange could have different effects on the T_2 observed. Secondly, the sampling time of the NMR CPMG sequence was considerably shorter than the minimum TE of the imaging sequence, thus making it possible to limit to a great extent diffusion effects. Note that chemical exchange also depended on TE. Differences were finally also due to the inevitable effects of contribution of the T_2 diffusion in the presence of imaging gradients. As in the phantom, tomato and apple tissue T_2 values were underestimated, and this phenomenon was amplified

for longer T_2, causing a reduction in the relaxation times measured in the MSE imaging experiment.

Another point to be considered is that the short sampling time of the NMR sequence used in combination with a long echo train (comparing to MRI sampling) might lead to a few discrepancies in the fitting results between the two techniques. The effects of the sampling were investigated on different sets of NMR transverse relaxation curves with echo times ranging from 1 ms to 11 ms. These curves were obtained by selecting specific points from the original relaxation curves measured in apple samples with echo time of 0.5 ms. The fitting results differed for fast relaxing components for which dispersion up to 20% in the T_2 values were observed without a distinct trend in the values. For other components, no changes were observed. No effects of echo train length on T_2 and associated relative signal intensities were observed in the specific case of the reconstructed NMR relaxation curve with similar echo time as this used in MRI experiments (7 ms) when only 512 points were used for fitting.

Analyses of the bi-compartment phantom showed that ROI fitting provided similar results to pixel-to-pixel fitting. However, for plant tissues exhibiting tri-exponential relaxation, an ROI-based approach became necessary to improve the SNR of the data. Although this approach does not provide fully spatially-resolved measurements, it renders multi-exponential relaxation parameter measurements possible without any sampling and keeps the measurements non-invasive. The relaxation times can be computed from the regions of interest drawn on homogeneous tissue regions of MRI images of the same size as samples used for NMR measurements. The sequence developed thus makes it possible to investigate changes in water status at a subcellular level without fruit sampling. Further developments will also focus on image processing methods for improvement of the signal-to-noise ratio of the images.

To the best of our knowledge, a tri-exponential T_2 fitting procedure in fruit tissues and the investigation of the effects of sequence parameters on multi-exponential T_2 measurements and its I_0 and T_2 distributions have not previously been performed using commercial MRI scanners. The approach could be extended from single slice study to 3D measurements.

In conclusion, the results of this study showed that the optimised MSE-MRI sequence can be used for up to tri-exponential T_2 quantification. The large number of points in the relaxation decay allows for estimation of relaxation times from a few tens of milliseconds to over a second, thus covering almost the entire range of transverse relaxation times in fruit cell compartments. Investigation of the effects of sequence parameters on multi-exponential T_2 and associated relative intensities showed that the sequence should be optimised with regard to the characteristics of the tissue to be examined. The effects of water molecular diffusion in the presence of both imaging gradients and gradients produced by susceptibility inhomogeneities have to be considered. This effect, which is pronounced in porous fruit tissues, means that only the shortest possible TE can be recommended.

LEGENDS:

Figure 1

A: Schematic representation of the bi-compartmental phantom used in the experiments. B: Positioning of the MRI imaging slice relative to the phantom for bi-exponential T_2 study.

Figure 2

MSE-MRI pulse sequence. Slice selection is performed by a soft 90° and then a train of hard 180° pulses repeated at TE intervals.

Figure 3

Effects of crusher in the phantom: (A) and (B) represent MSE amplitude images at TE = 12 ms in the absence of crusher and with the application of a crusher of 5 x 10^{-6} T.s/m, respectively. The T_2 values of the solutions are displayed on the images. (C) is the MRI signal decay plot of the solution with T_2 = 1392 ms through the 512 images. The signal is the mean value of the ROI shown on A and B.

Figure 4

Effects of crusher moment in the phantom: mean I_0 (A) and T_2 (B) values as a function of crusher moment for the mono-exponential decay measured in the phantom. (C) and (D) are the mean I_0 and T_2 values, respectively, as a function of crusher moment for the bi-exponential decay measured in the phantom. Vertical bars correspond to standard deviations. TE was set at 12 ms.

Figure 5

Effects of TE in the phantom: Mean I_0 (A) and T_2 (B) values as a function of TE for the mono-exponential decay measured in the phantom. (C) is the mean relative intensity signal of the pair of compartments with solutions of T_2 = [155/1392] ms. (D) represents T_2 values as a

function of TE in the bi-exponential configuration. A constant crusher of 5×10^{-6} T.s/m was used. Standard deviations are shown by vertical bars.

Figure 6

Effects of crusher moment in fruit tissues: Mean I_0 (A) and T_2 (B) values as a function of crusher moment in tomato tissue. (C) and (D) are the mean I_0 and T_2 values, respectively, of three different samples as a function of crusher moment in apple tissue. A constant TE of 12 ms was used. Standard deviations are shown with vertical bars.

Figure 7

Effects of TE in fruit tissues: a constant crusher of 5×10^{-6} T.s/m was used. Mean I_0 (A) and T_2 (B) values as a function of TE in tomato tissue. (C) and (D) are the mean I_0 and T_2 values, respectively, of three different samples as a function of TE in apple tissue. Standard deviations are shown with vertical bars.

Figure 8

(A) T_2-weighted images of the phantom (29th echo), (B) tomato (185th echo) and (C) apple (116th echo) obtained with MSE sequence; TE=7.1 ms, TR=10 s; crusher moment = 5×10^{-6} T.s/m and hard refocusing pulse. (D) Experimental points of the T_2 mean signal decays corresponding to the ROI shown in A $[T_{2,\,long}/T_{2,\,short}] = [596/155]$ and to the ROIs-1 shown in B and C. The plain curves represent the T_2 fits.

Figure 9

MRI-NMR I_0 (A) and T_2 (B) relationship plots of phantom and fruit tissues. TE = 7.1 ms and crusher moment = 5×10^{-6} T.s/m.

Figure 10

T_2 maps of the phantom in a bi-exponential configuration. (A) represents the relative signal intensities; and (B) and (C) are their corresponding T_2 values. Note that a defect in signal can be seen in (A) in the pair of tubes (second column, first row) with solutions of $T_2 = [32/1392]$ ms. This was most probably due to the bottom of the cavity of the phantom which was not perfectly flat.

Table 1

(A) NMR T_2 relaxation times and corresponding relative signal intensities of tomato and apple tissues obtained by discrete fitting method. Data were computed from the whole set of fruit samples. (B) Corresponding MRI results obtained with MSE sequence; TE=7.1 ms, TR=10 s; crusher moment = 5 x 10^{-6} T.s/m and hard refocusing pulse.

Table 2

Results of MRI T_2 measurements in the phantom solutions compared with NMR T_2 values. MRI measurements were performed with MSE sequence; TE=7.1 ms, TR=10 s; crusher moment = 5 x 10^{-6} T.s/m and hard refocusing pulse.

6 REFERENCES:

1. Hills BP, Clark CJ. Quality assessment of horticultural products by NMR. Annual Reports on NMR Spectroscopy 2003;50:75-120.
2. Borisjuk L, Rolletschek H, Neuberger T. Surveying the plant's world by magnetic resonance imaging. Plant Journal 2012;70(1):129-146.
3. Van As H, Scheenen T, Vergeldt FJ. MRI of intact plants. Photosynth Res 2009;102(2-3):213-222.
4. Clark CJ, MacFall JS. Quantitative magnetic resonance imaging of 'Fuyu' persimmon fruit during development and ripening. Magn Reson Imaging 2003;21(6):679-685.

5.   Musse M, Quellec S, Cambert M, Devaux M-F, Lahaye M, Mariette F. Monitoring the postharvest ripening of tomato fruit using quantitative MRI and NMR relaxometry. Postharvest Biol Technol 2009;53(1-2):22-35.

6.   Otero L, Prestamo G. Effects of pressure processing on strawberry studied by nuclear magnetic resonance. Innov Food Sci Emerg Technol 2009;10(4):434-440.

7.   Kotwaliwale N, Curtis E, Othman S, Naganathan GK, Subbiah J. Magnetic resonance imaging and relaxometry to visualize internal freeze damage to pickling cucumber. Postharvest Biology and Technology 2012;68:22-31.

8.   Van der Weerd L, Claessens M, Efde C, Van As H. Nuclear magnetic resonance imaging of membrane permeability changes in plants during osmotic stress. Plant Cell Environ 2002;25(11):1539-1549.

9.   Raffo A, Gianferri R, Barbieri R, Brosio E. Ripening of banana fruit monitored by water relaxation and diffusion H-1-NMR measurements. Food Chem 2005;89(1):149-158.

10.   Hills BP, Nott KP. NMR studies of water compartmentation in carrot parenchyma tissue during drying and freezing. Appl Magn Reson 1999;17(4):521-535.

11.   Hills BP, Remigereau B. NMR studies of changes in subcellular water compartmentation in parenchyma apple tissue during drying and freezing. International Journal of Food Science and Technology 1997;32(1):51-61.

12.   Saab G, Thompson RT, Marsh GD. Multicomponent T-2 relaxation of in vivo skeletal muscle. Magn Reson Med 1999;42(1):150-157.

13.   Donker HCW, Van As H, Edzes HT, Jans AWH. NMR imaging of white button mushroom (Agaricus bisporis) at various magnetic fields. Magnetic Resonance Imaging 1996;14(10):1205-1215.

14.   Haacke ME, Brown RW, Thompson MR, Venkatesan R. Magnetic Resonance Imaging. Physical Principles and Sequence Design: John Wiley and Sons; 1999. 914 p.

15.   Majumdar S, Orphanoudakis SC, Gmitro A, Odonnell M, Gore JC. Errors in the measurements of T2 using multiple-echo MRI techniques I. Effects of radiofrequency pulse imperfections. Magnetic Resonance in Medicine 1986;3(3):397-417.

16.   Majumdar S, Orphanoudakis SC, Gmitro A, Odonnell M, Gore JC. Errors in the measurements of T2 using multiple-echo MRI techniques II. Effects of static field inhomogeneity. Magnetic Resonance in Medicine 1986;3(3):562-574.

17.   Poon CS, Henkelman RM. Practical T2 quantitation for clinical applications. J Magn Reson Imaging 1992;2(5):541-553.

18.   Zur Y, Stokar S. A phase-cycling techique for cancelling spurious echoes in NMR imaging. Journal of Magnetic Resonance 1987;71(2):212-228.

19.   Crawley AP, Henkelman RM. Errors in T2 estimation using multislice multiple-echo imaging. Magnetic Resonance in Medicine 1987;4(1):34-47.

20.   Does MD, Gore JC. Complications of nonlinear echo time spacing for measurement of T-2. Nmr in Biomedicine 2000;13(1):1-7.

21.   LeBihan D. Molecular diffusion nuclear magnetic resonance imaging. Magn Res Q 1991;7(1):1-30.

22.   Edzes HT, van Dusschoten D, Van As H. Quantitative T2 Imaging of Plant Tissues By Means Of Multi-Echo MRI Microscopy. Magn Reson Imaging 1998;16(2):185-196.

23.   Majumdar S, Gore JC. Studies of Diffusion in Random-Fields Produced by Variations in Susceptibility. Journal of Magnetic Resonance 1988;78(1):41-55.

24.   Hills BP, Duce SL. The influence of chemical and diffusive exchange on water proton transverse relaxation in plant tissues. Magnetic Resonance Imaging 1990;8(3):321-331.

25. Musse M, Cambert M, Mariette F. NMR Study of Water Distribution inside Tomato Cells: Effects of Water Stress. Appl Magn Reson 2010;38(4):455-469.
26. Musse M, Quellec S, Devaux M-F, Cambert M, Lahaye M, Mariette F. An investigation of the structural aspects of the tomato fruit by means of quantitative nuclear magnetic resonance imaging. Magn Reson Imaging 2009;27(5):709-719.
27. Carr HY, Purcell EM. Effects of Diffusion on Free Precession in Nuclear Magnetic Resonance experiments. Phys Rev 1954;94(3):630-638.
28. Meiboom S, Gill D. Modified Spin-Echo Method for Measuring Nuclear Relaxation Times. Rev Scient Instr 1958;29:688-691.
29. Mariette F, Guillement JP, Tellier C, Marchal P. Continuous relaxation time distribution decomposition by MEM. In: Rutledge DN, editor. Signal Treatment and Signal Analysis in NMR. Paris: Elsevier; 1996. p 218-234.
30. Sibgatullin TA, Anisimov AV, de Jager PA, Vergeldt FJ, Gerkema E, Van As H. Analysis of diffusion and relaxation behavior of water in apple parenchymal cells. Biofizika 2007;52(2):268-276.
31. Musse M, De Guio F, Quellec S, Cambert M, Challois S, Davenel A. Quantification of microporosity in fruit by MRI at various magnetic fields: comparison with X-ray microtomography. Magn Reson Imaging 2010;28(10):1525-1534.
32. Sled JG, Pike B. Correction for B1 and B0 Variations in Quantitative T2 Measurements Using MRI. Magn Reson Med 2000;43:589–593.
33. Prasloski T, Maedler B, Xiang Q-S, MacKay A, Jones C. Applications of stimulated echo correction to multicomponent T2 analysis. Magn Reson Med 2012;67(6):1803-1814.
34. Dula AN, Gochberg DF, Does MD. Optimal echo spacing for multi-echo imaging measurements of Bi-exponential T(2) relaxation. J Magn Reson 2009;196(2):149-156.
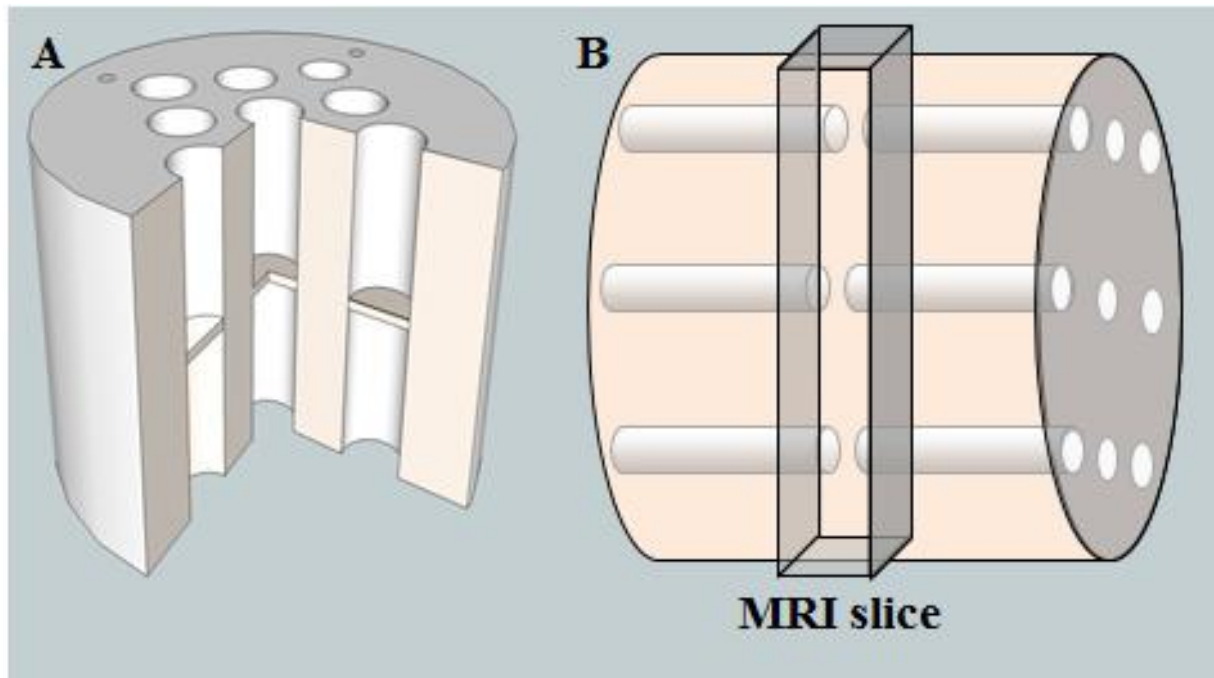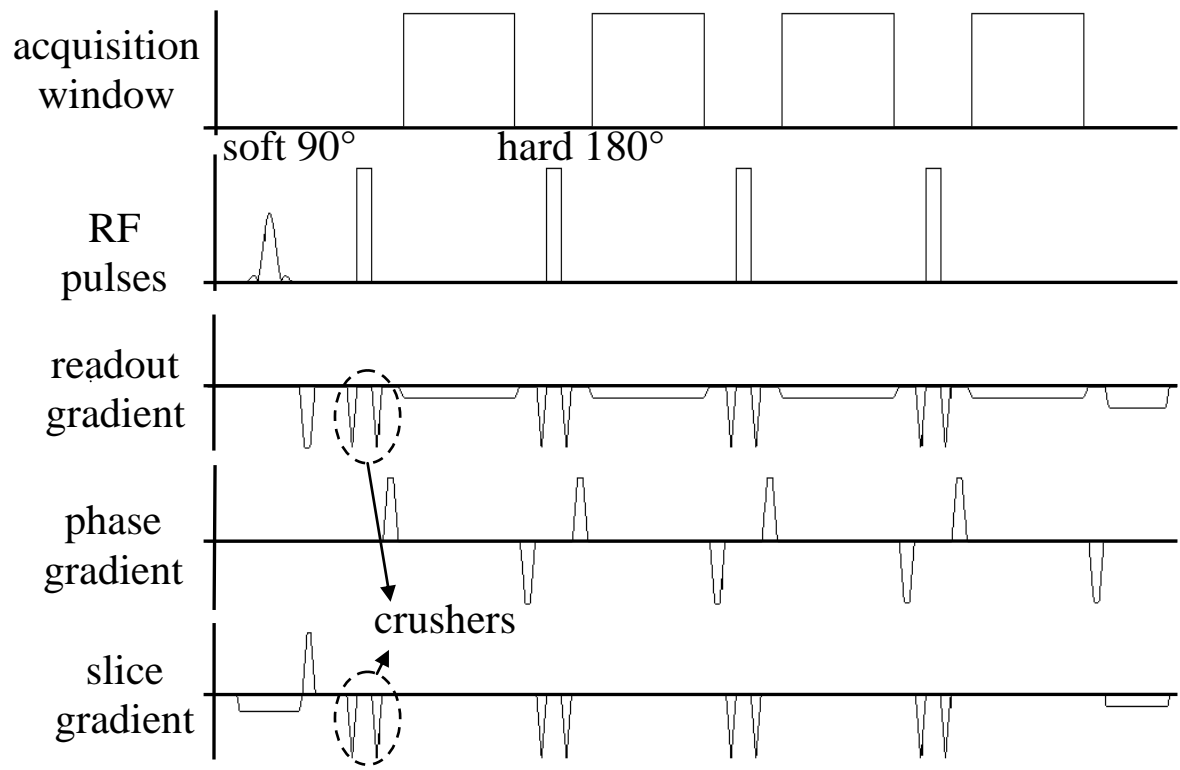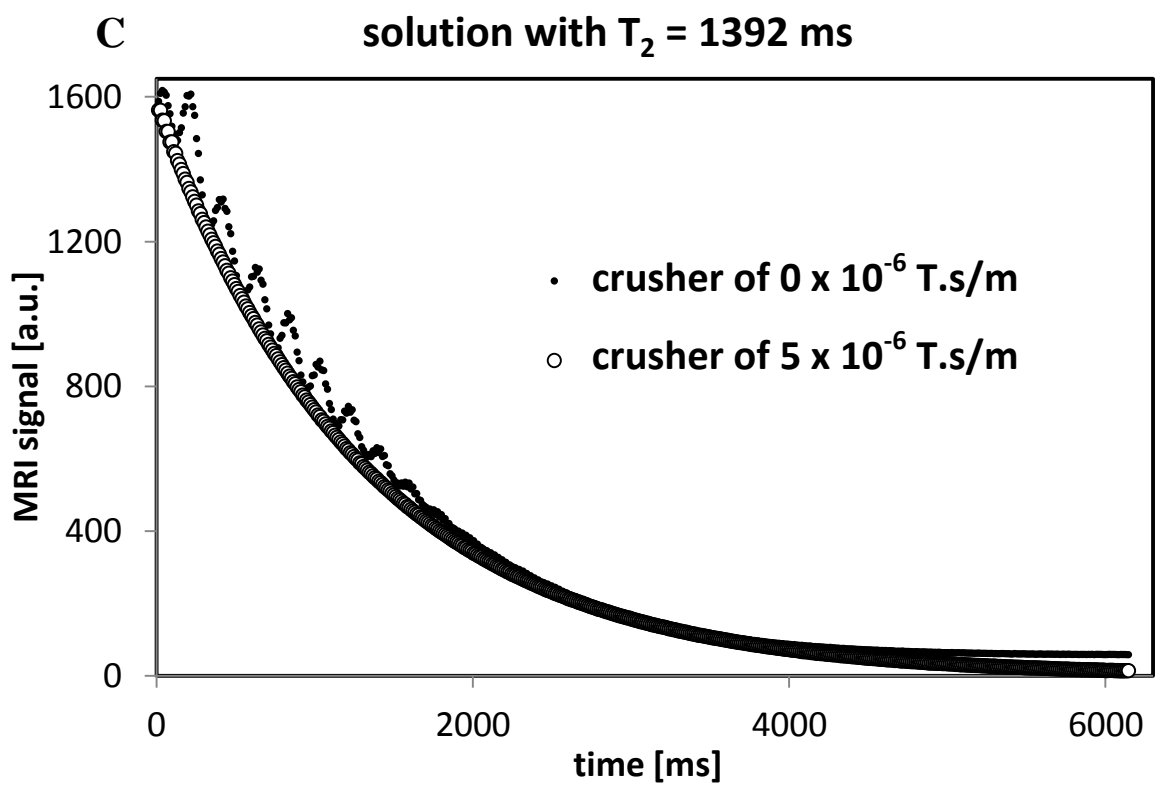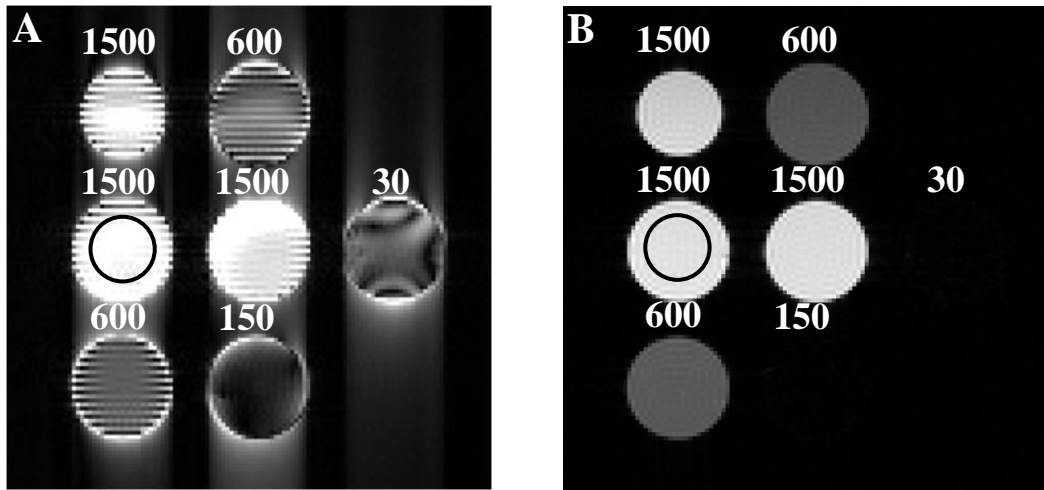
Figure 1

Figure 2

acquisition
window

soft 90°   hard 180°

RF
pulses

readout
gradient

phase
gradient

crushers

slice
gradient

Figure 3

Figure 4

Figure 5

A

mono-exponential

B

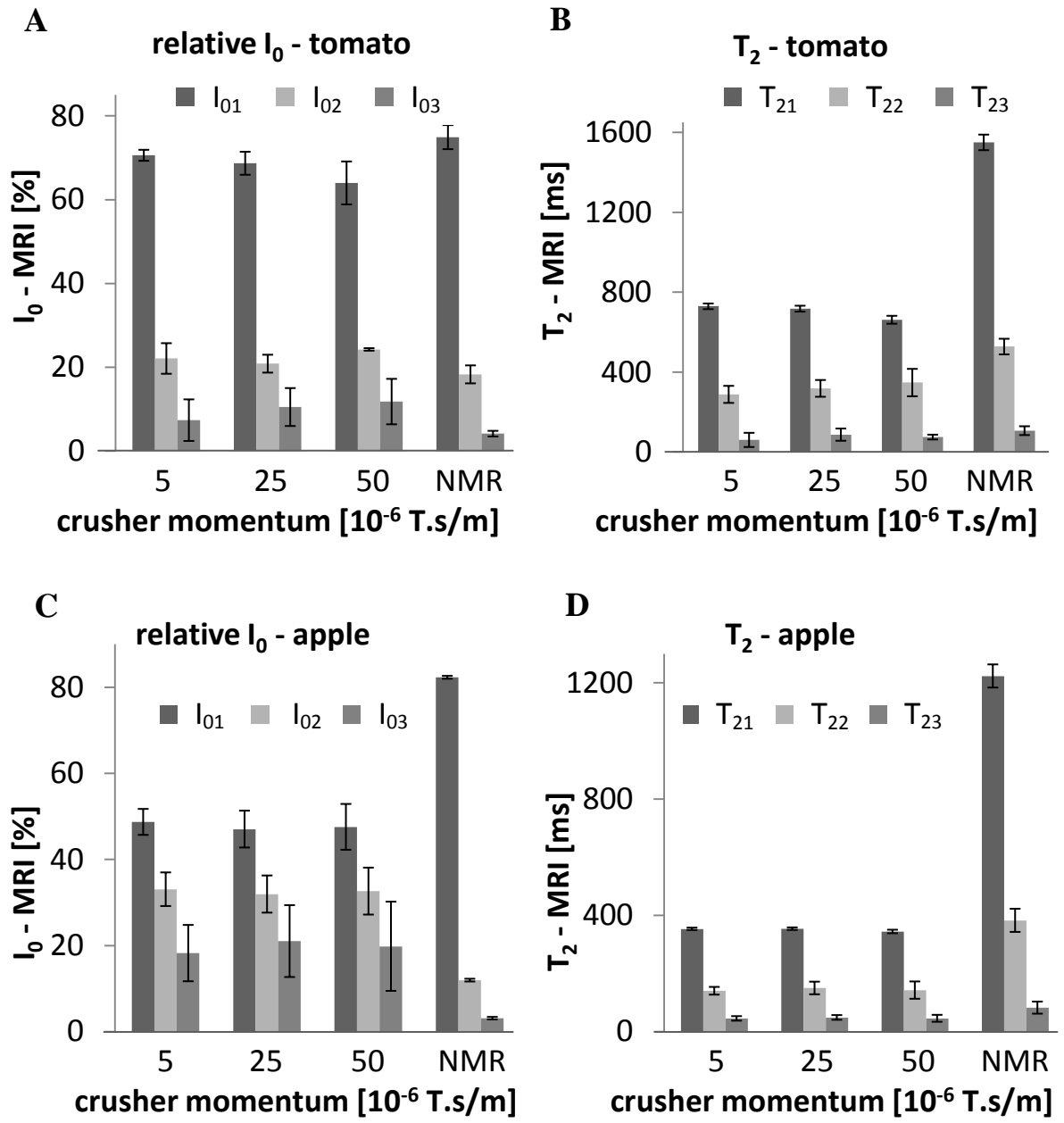**mono-exponential**

C

bi-exponential

D

bi-exponential
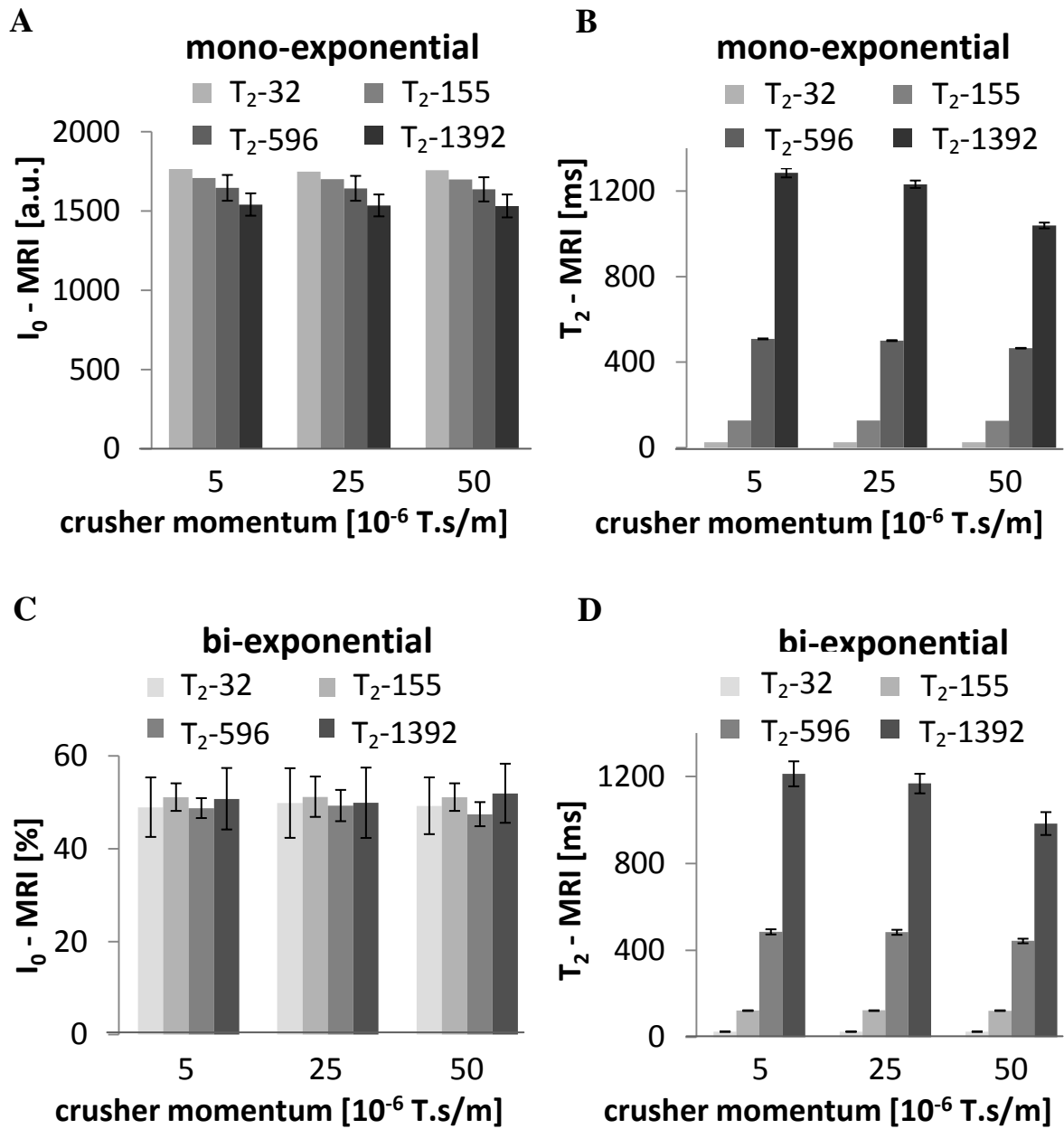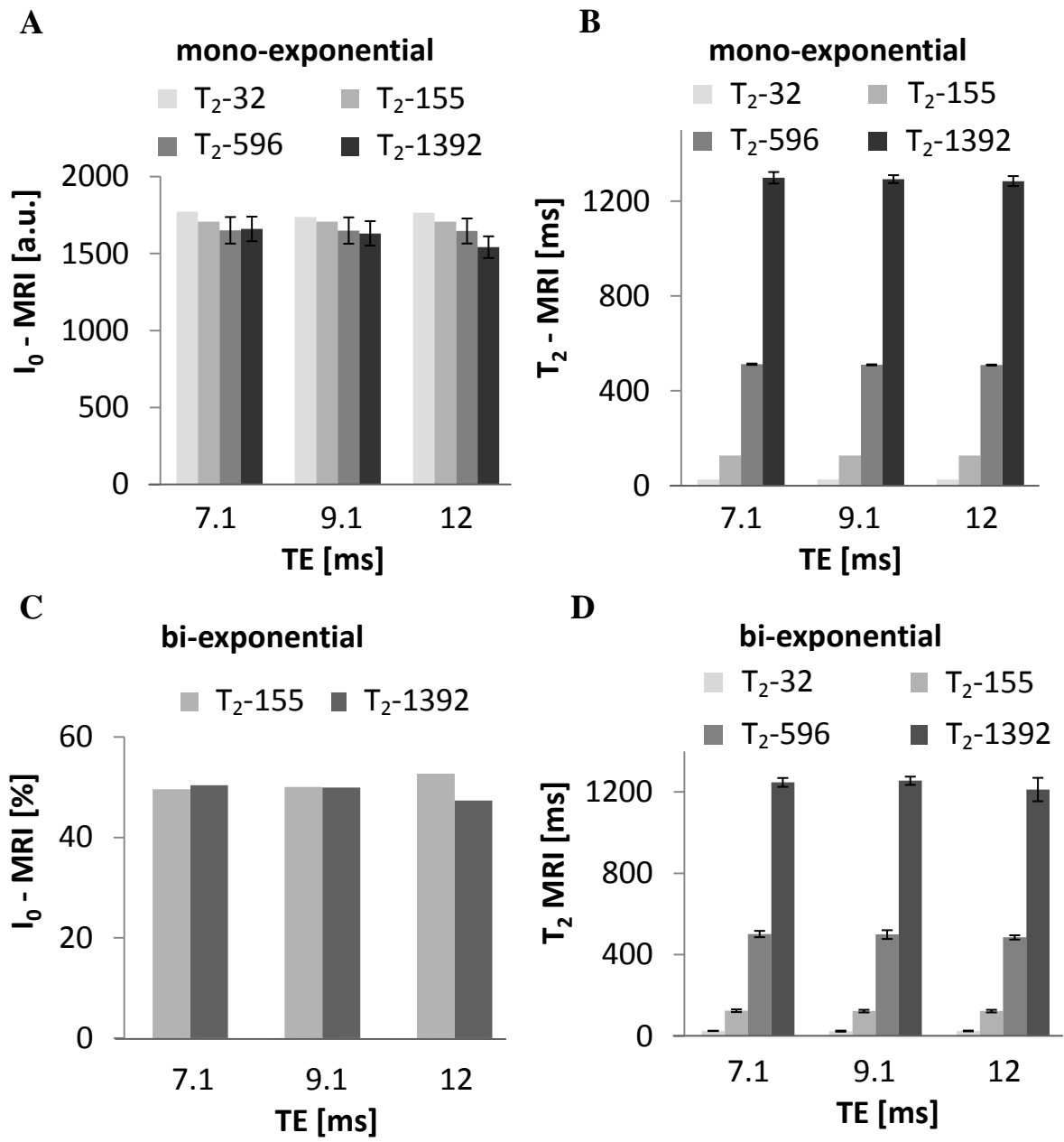
Figure 6

Figure 7
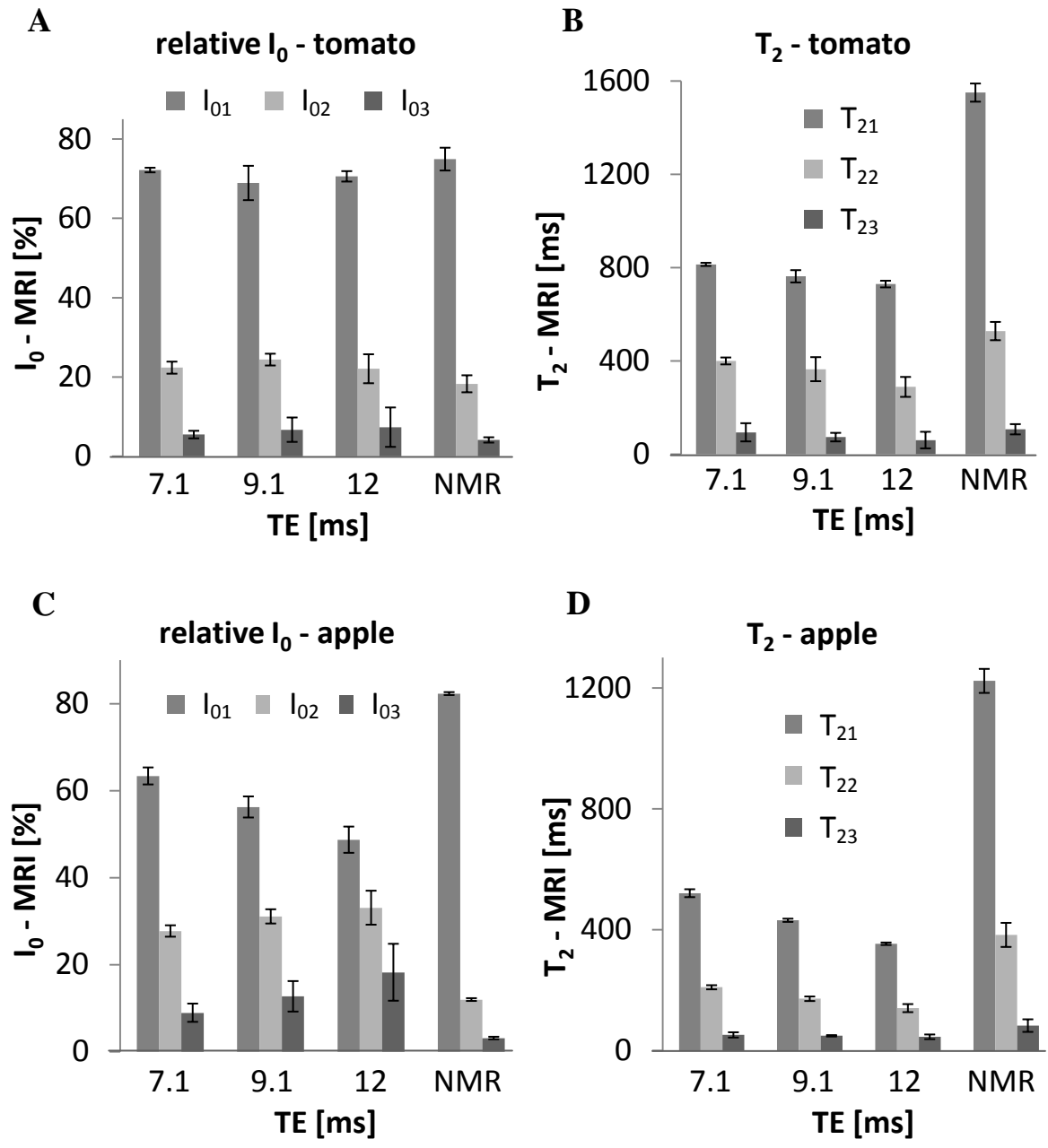
Figure 8
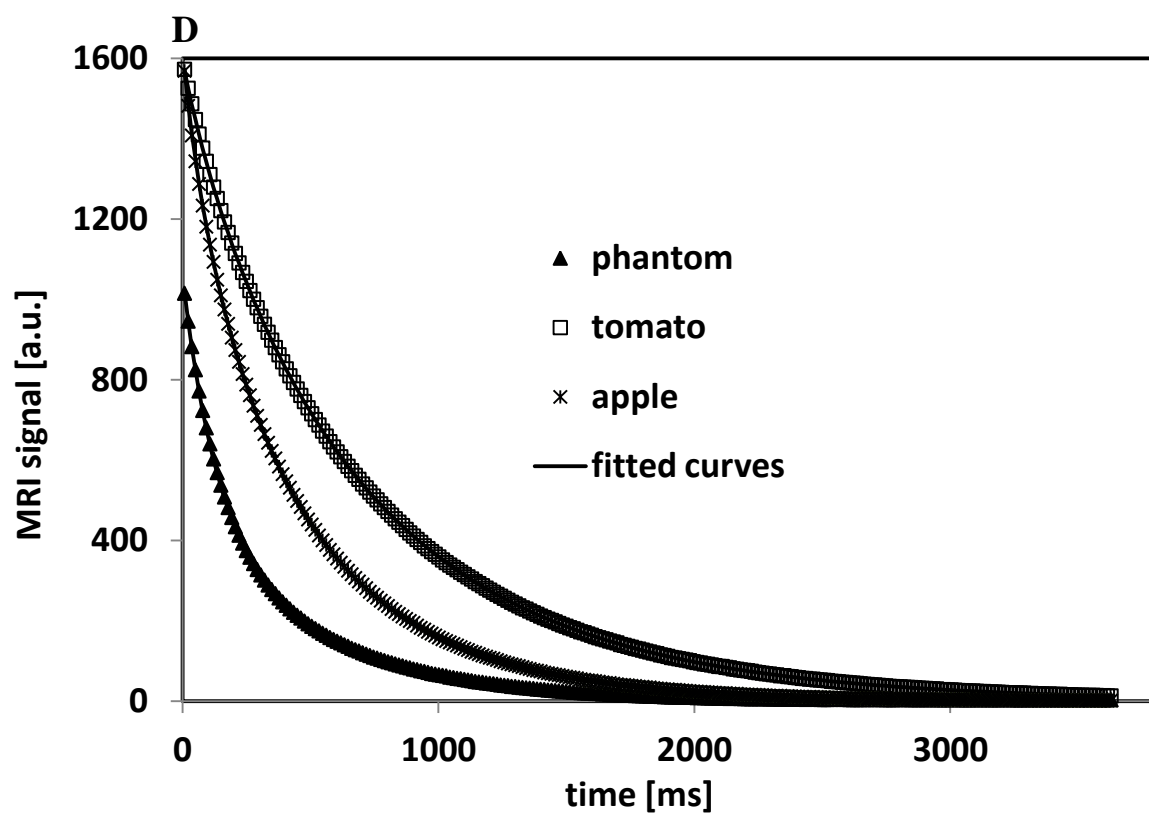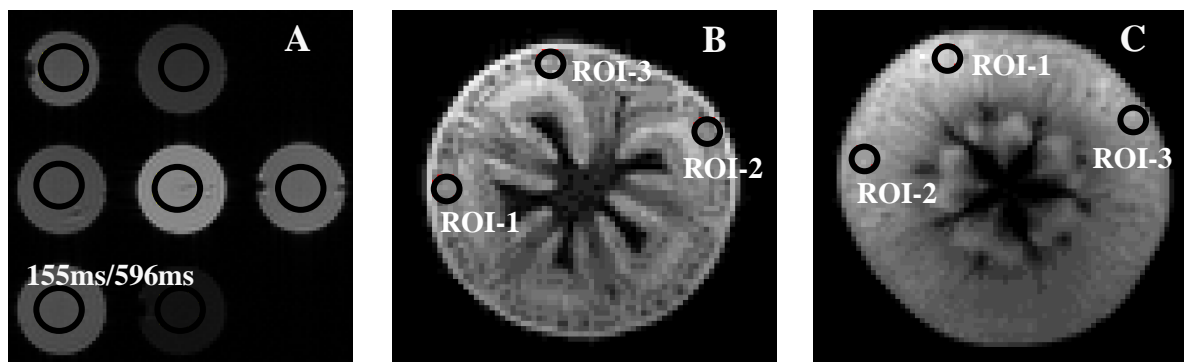
Figure 8

Figure 9

Figure 10
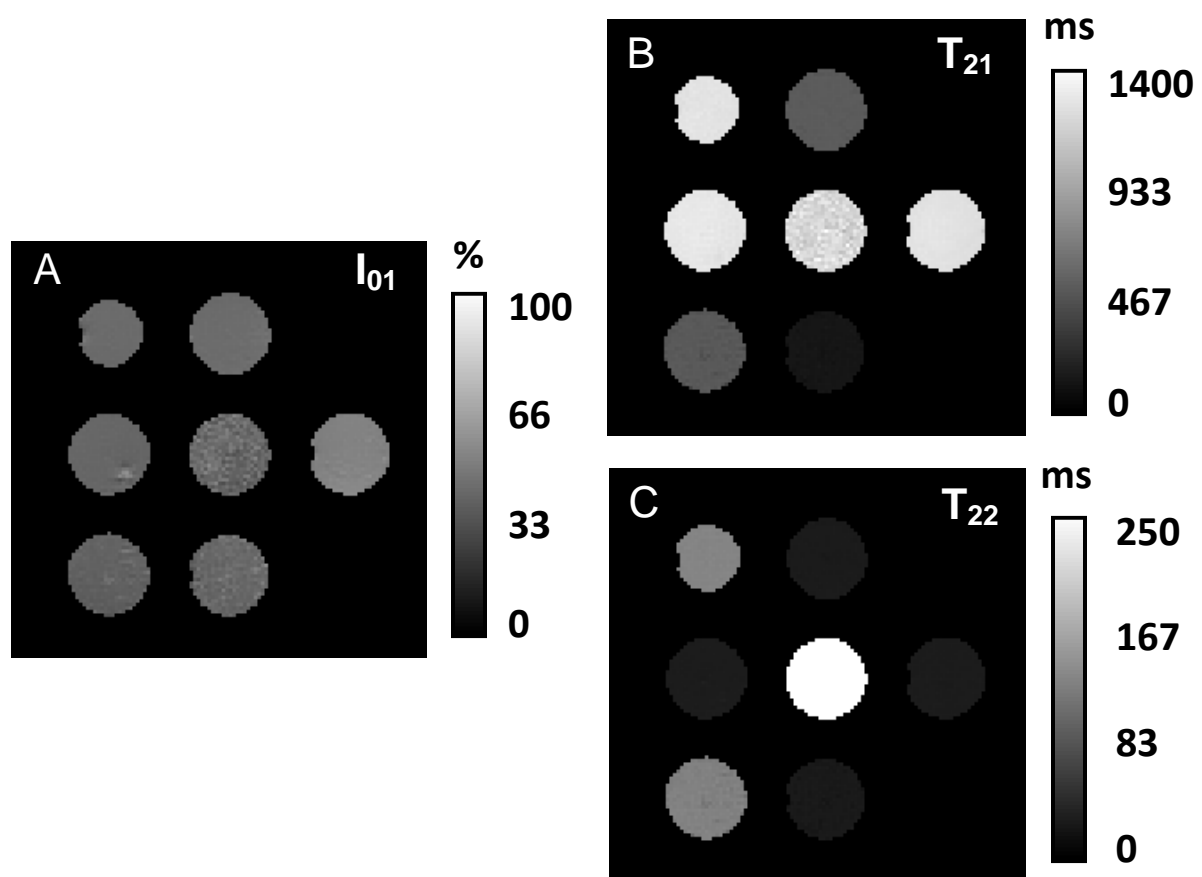
Table 1

(A)

	COMPONENT 1		COMPONENT 2		COMPONENT 3		COMPONENT 4	
	T_{21} [ms]	I_{01} [%]	T_{22} [ms]	I_{02} [%]	T_{23} [ms]	I_{03} [%]	T_{24} [ms]	I_{04} [%]
TOMATO	1578±65	71±5	577±69	21±4	123±26	5±1	16±3	2.9±0.4
APPLE	1228±39	81±1	376±27	13±1	88±13	3.1±0.4	10±2	3.0±0.3

(B)

	COMPONENT 1		COMPONENT 2		COMPONENT 3	
	T_{21} [ms]	I_{01} [%]	T_{22} [ms]	I_{02} [%]	T_{23} [ms]	I_{03} [%]
TOMATO	835±66	67±6	455±60	26±5	114±41	6±2
APPLE	506±29	64±5	207±22	27±3	53±10	8±2

Table 2

T_2 – NMR [ms]	1392±9	596±3	155±1	32±0
T_2 – MRI [ms]	1248±22	502±16	125±7	26±1